



**HAL**  
open science

## Current and optimal dimensions predictions for a porous micro-electrode

Tien D Le, Didier Lasseux

► **To cite this version:**

Tien D Le, Didier Lasseux. Current and optimal dimensions predictions for a porous micro-electrode. ChemElectroChem, 2020, 7 (14), pp.3017-3027. hal-03042091

**HAL Id: hal-03042091**

**<https://hal.science/hal-03042091>**

Submitted on 5 Dec 2020

**HAL** is a multi-disciplinary open access archive for the deposit and dissemination of scientific research documents, whether they are published or not. The documents may come from teaching and research institutions in France or abroad, or from public or private research centers.

L'archive ouverte pluridisciplinaire **HAL**, est destinée au dépôt et à la diffusion de documents scientifiques de niveau recherche, publiés ou non, émanant des établissements d'enseignement et de recherche français ou étrangers, des laboratoires publics ou privés.

1 Current and optimal dimensions predictions for a  
2 porous micro-electrode

3 Tien D. Le \*      Didier Lasseux<sup>†</sup>

4 **1 Abstract**

5 The expression of the current delivered by a cylindrical porous micro-electrode  
6 operating a single heterogeneous reaction and mass diffusion of the reagent is  
7 analytically derived in this work from a *complete solution* of the diffusion/reaction  
8 macroscopic problem. This solution is valid regardless of the aspect (thickness  
9 to inner radius) ratio. It encompasses the *hybrid solution* reported elsewhere,  
10 valid only when this ratio remains small compared to unity, and, consequently,  
11 the case of a planar electrode as well. The asymptotic form of the solution in  
12 this latter case is also provided. The complete solution is used to predict the  
13 optimal thickness of the electrode and its optimal inner radius (*i.e.* the sup-  
14 porting wire radius) corresponding to the best compromise between a minimum  
15 electrode volume and a maximum current per unit volume. This work hence  
16 provides a complete optimization procedure that can be used as predictive tools  
17 for the design of porous electrodes.

18 **2 Introduction**

19 The development of miniaturized electrodes has been the subject of intense in-  
20 terest for the past decade, in particular for bio-implantable electro-devices.<sup>[1]</sup>  
21 In order to reduce their size, micro- or nanoporous materials are particularly  
22 attractive due to their high specific surface area available for the heterogeneous  
23 redox reactions, hence producing a much larger current than a flat electrode  
24 of the same size.<sup>[2]</sup> An abundant literature has been dedicated to the study of  
25 these devices, both from theoretical and experimental points of view. Many dif-  
26 ferent operating conditions can be envisaged for these electrodes<sup>[3,4,5,6]</sup>, namely  
27 without any catalyst<sup>[7,8]</sup> or with an embedded enzyme to catalyze the redox re-  
28 actions which may occur in the direct electron transfer<sup>[9]</sup> or mediated electron

---

\*Dr. Tien D. Le I2M, UMR 5295, CNRS, Univ. Bordeaux, Esplanade des Arts et Métiers,  
33405 Talence CEDEX, France - Université de Lorraine, CNRS, LEMTA, F-54000 Nancy,  
France

<sup>†</sup>Dr. Didier Lasseux I2M, UMR 5295, CNRS, Univ. Bordeaux, Esplanade des Arts et  
Métiers, 33405 Talence CEDEX, France - Corresponding author: didier.lasseux@u-bordeaux.fr

29 transfer mode.<sup>[10]</sup> A classical procedure to obtain a porous material relies on  
30 a Langmuir-Blodgett templating method related to self-assembly of particles.  
31 This is followed by electrodeposition of a conducting material. After dissolving  
32 the particles, a synthetic porous electrode composed of interconnected pores is  
33 obtained which porosity and internal architecture can be tuned.<sup>[11,12,2]</sup>

34 The coupled process of transport and electrochemical reaction occurring  
35 during voltammetry experiments for porous electrodes has been modelled in  
36 both cases with or without catalysis.<sup>[13,14,15]</sup> Recently, a multiscale model for  
37 a porous electrode operating a single reaction was developed<sup>[7]</sup>, providing a  
38 macroscopic model and a closure problem which solution allows to determine  
39 the effective parameter (effective diffusion coefficient). Such a model was val-  
40 idated by comparing its predictions with 3D direct numerical simulations at  
41 the pore scale similar to those reported recently.<sup>[16]</sup> It was also successfully  
42 compared with experimental data. The advantage of such an approach is that  
43 the ensuing macroscale model, which contains the necessary information from  
44 the microscale, is much simpler to solve than the original one at the scale of  
45 the microstructure, avoiding cumbersome direct numerical simulations at this  
46 scale. Further, an optimization procedure, based on the macroscopic model to  
47 estimate the optimal thickness of cylindrical porous electrodes, has been inves-  
48 tigated.<sup>[17]</sup> It was derived under the assumption that the electrode thickness is  
49 much smaller than its inner radius, although the diffusion layer thickness sur-  
50 rounding the electrode is not. This yielded the so-called *hybrid model*. However,  
51 such an assumption can fail in practice and it is hence of major interest to derive  
52 a prediction of the optimal thickness in the general case.

53 In the present work, an accurate *complete solution* of the upscaled model  
54 in its general form is proposed in order to predict the current delivered by a  
55 cylindrical electrode in the steady regime and to estimate its optimal thickness  
56 and optimal inner radius without any assumption on its microstructure and  
57 dimensions. This solution is expressed in terms of the Bessel's functions of the  
58 first and second kinds; it is valid whatever the thickness to inner radius ratio  
59 and is hence general.

60 Predictions of this model are compared to those obtained from the hybrid  
61 model in the case of a face-centered cubic, cubic and body-centered cubic struc-  
62 tures of the porous material. Moreover, an analytical solution is also derived for  
63 planar electrodes which conveniently matches the complete solution for cylindri-  
64 cal electrodes in the limit of an extremely large radius compared to the thickness.  
65 Finally, the optimal radius of the supporting wire that leads to the minimum  
66 volume of the electrode is derived. This represents a very important result,  
67 leading to a complete optimization process of the macroscopic dimensions of  
68 the electrode.

69 The paper is organized as follows. In Section 2, the upscaled model for the  
70 coupled electrochemical reaction and transport in a porous micro-electrode is  
71 briefly recalled. A complete analytical solution of the macroscopic model for  
72 a cylindrical geometry is proposed in Section 3 without any restriction on the  
73 electrode dimensions. Such a solution is compared to that of the hybrid model  
74 developed in<sup>[17]</sup> to predict the optimal electrode thickness. In Section 4, an

75 analytical solution of the macroscopic model and for the optimal thickness of  
 76 a planar electrode is proposed. Section 5 is dedicated to the derivation of the  
 77 optimal radius of the cylindrical wire supporting the electrode, which, along  
 78 with its optimal thickness, provides a complete framework for its macroscopic  
 79 optimization. Concluding remarks are drawn in Section 6.

### 80 3 Recall of the upscaled model

In this section, the upscaled model for a porous electrode operating a single reduction reaction, as proposed in previous works<sup>[7,17]</sup>, is briefly recalled to further develop its solution. This model is derived from the pore-scale initial boundary value problem (IBVP) describing the coupled diffusion and heterogeneous reaction of the species of interest. Diffusion of this species,  $A$ , (of molar concentration  $c_A$ ) dissolved in the solution saturating the electrode's pore space, denoted  $\Omega_f$ , is governed by Fick's law.<sup>[18]</sup> It is beyond the scope of this article to provide the details for this governing law to apply here. The reader is referred to<sup>[19]</sup> for the assumptions and constraints that support it. At the pore solid/fluid interfaces,  $\mathcal{I}_{sf}$ , a single reaction reducing  $A$  to  $B$  is considered for which the electron transfer mechanism is described by the Butler-Volmer's relation<sup>[20]</sup> (see Fig. 1). The IBVP at the pore scale can be formulated as follows

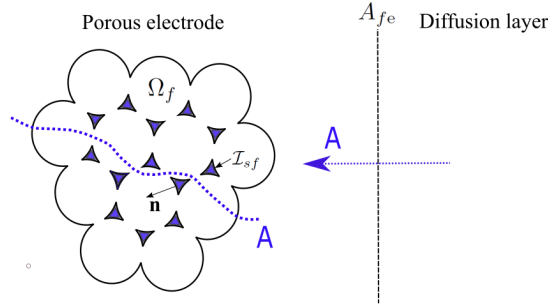


Figure 1 – Pore-scale configuration.

$$\frac{\partial c_A}{\partial t} = \nabla \cdot (\mathcal{D}_A \nabla c_A) \quad \text{in } \Omega_f \quad (1a)$$

$$\text{B.C.1} \quad -\mathbf{n} \cdot \mathcal{D}_A \nabla c_A = k_0 \alpha_A c_A \quad \text{at } \mathcal{I}_{sf} \quad (1b)$$

$$\text{B.C.2} \quad c_A = \mathcal{G}_A(\mathbf{r}, t) \quad \mathbf{r} \in A_{fe}, \forall t \quad (1c)$$

$$\text{I.C.} \quad c_A = \mathcal{F}_A(\mathbf{r}) \quad \mathbf{r} \in \Omega_f, t = 0 \quad (1d)$$

81 In these equations,  $\mathcal{D}_A$  is the molecular diffusion coefficient of species  $A$ ,  $\mathbf{n}$   
 82 denotes the unit normal vector at  $\mathcal{I}_{sf}$ , pointing out of  $\Omega_f$ , and  $k_0$  is the standard  
 83 rate constant of the reaction. Moreover,  $\alpha_A = \exp\left(\frac{-\alpha n F (E - E^0)}{RT}\right)$  where  $\alpha$ ,

84  $n$ ,  $E$  and  $E^0$  are the electron transfer coefficient, the number of transferred  
 85 electrons, the electrode potential and the standard potential respectively,  $F$ ,  $R$   
 86 and  $T$  representing the Faraday's constant, ideal gas constant and temperature.  
 87 In this work,  $T$  is assumed to be constant and the conduction of electrons in the  
 88 solid phase is supposed to be extremely fast so that the potential in this phase  
 89 can be readily considered as uniform. It should be noted that in the boundary  
 90 condition B.C.2,  $A_{fe} = \Omega_f \cap \Omega_e$  is the entrance and/or exit boundaries of the  
 91 fluid phase,  $\Omega_f$ , from/into the diffusion layer surrounding the electrode, denoted  
 92  $\Omega_e$ .

The above pore-scale IBVP can be upscaled using the volume averaging method<sup>[21]</sup> to obtain a model at the macroscopic scale. To do so, a separation of length-scales is assumed between the characteristic pore length-scale,  $\ell_p$ , and the characteristic macroscopic length scale,  $L$ , of the system. In addition, it is assumed that an intermediate scale  $r_0$  can be exhibited satisfying  $\ell_p \ll r_0 \ll L$  such that an averaging domain,  $\mathbf{V}$ , of measure  $V$  and size  $r_0$  can be used to average the pore-scale IBVP. The domain  $\mathbf{V}$  is usually chosen so as to contain all the necessary microstructural information in order to be a representative elementary volume (REV) of the porous medium and the physical process at play. In this way, the macroscopic model is expressed in terms of the intrinsic average concentration of species  $A$ , denoted  $\langle c_A \rangle^f$ . It is defined in  $\mathbf{V}$  in which the fluid phase occupies a domain  $\mathbf{V}_f$ , of measure  $V_f$ , as

$$\langle c_A \rangle^f = \frac{1}{V_f} \int_{\mathbf{V}_f(\mathbf{x})} c_A dV \quad (2)$$

The averaging procedure is then carried out in three main steps. The averaging operator of Eq. (2) is first applied to the pore-scale IBVP, and in order to interchange time and space derivations with integration, the general transport theorem<sup>[22]</sup> and the averaging theorem<sup>[23]</sup> are employed. When the porous medium is rigid and homogeneous, they can be respectively expressed as

$$\left\langle \frac{\partial \psi}{\partial t} \right\rangle^f = \frac{\partial \langle \psi \rangle^f}{\partial t} \quad (3a)$$

$$\langle \nabla \psi \rangle^f = \nabla \langle \psi \rangle^f + \frac{1}{V_f} \int_{\mathcal{A}_{sf}} \mathbf{n} \psi dA \quad (3b)$$

93 In the latter,  $\mathcal{A}_{sf}$ , of measure  $A_{sf}$ , represents the portion of  $\mathcal{I}_{sf}$  contained in  $\mathbf{V}$ .  
 94 In a second step, the physical variables  $\psi$  (here  $\psi = c_A$ ) are spatially decomposed  
 95 under the form  $\psi = \langle \psi \rangle^f + \tilde{\psi}$ <sup>[24]</sup>,  $\tilde{\psi}$  representing the spatial fluctuations of  $\psi$  with  
 96 respect to its average  $\langle \psi \rangle^f$ . This decomposition is introduced in the averaged  
 97 equations which can be usually simplified on the basis of the scale hierarchy.  
 98 This yields an unclosed model in which both  $\langle \psi \rangle^f$  and  $\tilde{\psi}$  are present. In a  
 99 third step, the (initial) boundary value problem for  $\tilde{\psi}$  is derived and this is  
 100 obtained by subtracting the unclosed macroscopic equations from their pore-  
 101 scale analogues. The equations for  $\tilde{\psi}$  are then simplified on the basis of the

102 length scale constraints. These constraints further allow obtaining a formal  
 103 solution expressed in terms of *closure variables* by making the problem on  $\tilde{\psi}$   
 104 periodic over a periodic unit cell, at least as large as the REV. For simplicity,  
 105 this periodic unit cell is identified as the REV in the remainder of this work.  
 106 The formal solution for  $\tilde{\psi}$  is introduced in the unclosed macroscopic equations,  
 107 on the one hand, and in the problem for  $\tilde{\psi}$ , on the other hand, yielding the  
 108 closed macroscopic model and the *closure problem(s)* for the closure variables,  
 109 respectively. The closed model involves effective coefficients that are determined  
 110 from the solution of the closure problem(s).

111 When the procedure described above is applied to the IBVP in Eqs. (1), the  
 112 following macroscopic mass conservation equation is obtained<sup>[7,17]</sup>

$$\epsilon_f \frac{\partial \langle c_A \rangle^f}{\partial t} = \nabla \cdot \left( \epsilon_f \mathbf{D}_{eff} \cdot \nabla \langle c_A \rangle^f \right) - k_0 \alpha_A a_v \langle c_A \rangle^f \quad \text{in } \Omega \quad (4)$$

Here,  $\Omega$  denotes the macroscopic domain occupied by the electrode whereas  $\epsilon_f$   
 and  $a_v$  are the porosity and specific area, respectively defined by

$$\epsilon_f = \frac{V_f}{V}; \quad a_v = \frac{A_{sf}}{V} \quad (5)$$

In addition, in Eq. (4),  $\mathbf{D}_{eff}$  is the effective diffusion tensor which is computed  
 from the solution of an intrinsic closure problem in a periodic REV (see Eqs.  
 (16) reported in a previous work.<sup>[7]</sup>) An example of a REV, of size  $\ell_R \equiv r_0$ , is  
 depicted in Fig. 2 for a FCC structure constitutive of a porous electrode. It

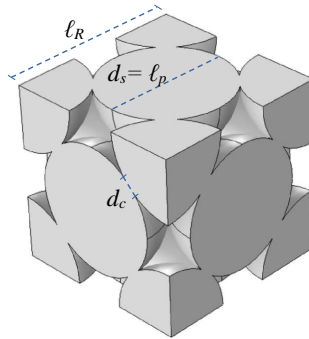


Figure 2 – Unit cell of a FCC structure with the characteristic dimensions. The gray area corresponds to the fluid domain while the solid phase is not represented. Spherical pores are connected through windows of diameter  $d_c$ .

should be noted that the second term on the right hand side of Eq. (4) originates  
 from the heterogeneous reduction reaction of species  $A$  indicated in the pore-  
 scale boundary condition in Eq. (1b) that is now reflected in the macroscopic  
 mass conservation equation. The current delivered by the electrode can then be  
 expressed from the average concentration as<sup>[7]</sup>

$$I = -nk_0 F \alpha_A a_v \int_{\Omega} \langle c_A \rangle^f dV \quad (6)$$

113 To obtain the solution on  $\langle c_A \rangle^f$  in  $\Omega$ , macroscopic boundary and initial con-  
 114 ditions corresponding to the pore-scale analogues in Eqs. (1c) and (1d) must  
 115 be specified. In practice, the electrode is immersed in the fluid saturating the  
 116 pores. The mass transfer of species  $A$  in the surrounding bulk fluid, which is  
 117 assumed to obey Fick's second law (Eq. (1a)), gives rise to a diffusion layer, of  
 118 thickness  $L_N$ , next to the fluid-electrode boundary. The concentration at the  
 119 outer edge of this boundary layer remains constant over time and is denoted  $c_A^0$   
 120 which is assumed to be the uniform concentration value in the whole system at  
 121  $t = 0$ . At the boundary between the electrode and the diffusion layer, continu-  
 122 ity of both the concentration and the flux can be reasonably assumed as was  
 123 investigated earlier.<sup>[7]</sup> A resistance to mass transfer may be considered at the  
 124 fluid-electrode boundary. However, this mechanism would contribute to hinder  
 125 the penetration of species  $A$  inside the electrode and would hence lead to predict  
 126 an optimal thickness smaller than that in the absence of this mechanism. In the  
 127 following the existence of mass transfer resistance is ignored with the idea that  
 128 this leads to the maximum expected value of the optimal electrode thickness.  
 129 Moreover, in order to determine this optimal thickness, the stationary regime  
 130 is to be considered for which the penetration depth of the diffusion/reaction  
 131 front has settled down inside the electrode.

132 The solution of the coupled diffusion-reaction macroscopic equation (4), con-  
 133 sidering the diffusion layer in the bulk fluid next to  $\Omega$ , was proposed for a  
 134 cylindrical electrode in the stationary regime.<sup>[17]</sup> However, this solution was  
 135 restricted to the case where the thickness of the electrode remains small com-  
 136 pared to its inner radius, although this assumption may not apply to the outer  
 137 boundary layer thickness. This led to a so-called hybrid model. In practice,  
 138 the electrode can be thick enough for this assumption to fail and it is hence of  
 139 major importance to reconsider the problem in a more general case by deriving  
 140 a solution referred to as the complete solution (or *Bessel's solution*). This is  
 141 the purpose of the following section.

## 142 4 Cylindrical electrode

143 The cylindrical electrode under consideration is made of a porous material de-  
 144 posited on a conducting cylindrical wire of radius  $R_1$ . Its thickness is  $L_e$  and  
 145 its external radius  $R_2 = R_1 + L_e$ . The diffusion layer outside the electrode is  
 146 supposed to have an external radius  $R_3 = R_2 + L_N$ . A schematic cross section of  
 147 the configuration, with the normalized characteristic radial dimensions denoted  
 148 with the superscript  $*$ , is depicted in Fig. 3. The reference dimension used to  
 149 normalize the radial coordinate is the characteristic size,  $\ell_R$ , of the periodic unit  
 150 cell (the REV) of the porous medium. The wire center is positioned at  $r^* = 0$ .

Using the initial concentration  $c_A^0$ , that is supposed to be uniform in the  
 whole system at  $t = 0$ , as the reference concentration, and assuming that steady

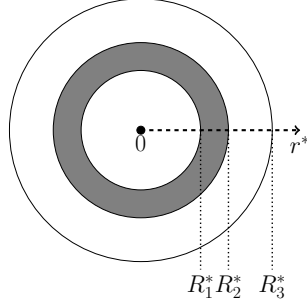


Figure 3 – Cross section of a cylindrical electrode of external dimensionless radius  $R_2^*$  made of a porous material (gray area) deposited on a cylindrical wire of dimensionless radius  $R_1^*$  and surrounded by the diffusion layer which external dimensionless radius is  $R_3^*$ .

state is reached, the macroscale problem takes the following form

$$r^{*2} \frac{d^2 \langle c_A^* \rangle^f}{dr^{*2}} + r^* \frac{d \langle c_A^* \rangle^f}{dr^*} = \varphi^2 r^{*2} \langle c_A^* \rangle^f \quad R_1^* \leq r^* \leq R_2^* \quad (7a)$$

$$\frac{d}{dr^*} \left( r^* \frac{dc_A^*}{dr^*} \right) = 0 \quad R_2^* \leq r^* \leq R_3^* \quad (7b)$$

$$\text{B.C.1: } D_{eff}^* \frac{d \langle c_A^* \rangle^f}{dr^*} = \frac{dc_A^*}{dr^*} \quad r^* = R_2^* \quad (7c)$$

$$\text{B.C.2: } \langle c_A^* \rangle^f = c_A^* \quad r^* = R_2^* \quad (7d)$$

$$\text{B.C.3: } \frac{d \langle c_A^* \rangle^f}{dr^*} = 0 \quad r^* = R_1^* \quad (7e)$$

$$\text{B.C.4: } c_A^* = 1 \quad r^* = R_3^* \quad (7f)$$

In B.C.1 and B.C.2, continuity of both the flux and the concentration is assumed at the porous electrode-diffusion layer interface ( $r^* = R_2^*$ ). At the electrode-wire interface,  $r^* = R_1^*$ , a zero flux is considered whereas a Dirichlet boundary condition is used at the external boundary of the diffusion layer ( $r^* = R_3^*$ ) where the initial concentration,  $c_A^0$ , is imposed. In Eq. (7c),  $D_{eff}^* = \varepsilon_f D_{eff} / \mathcal{D}_A$ , ( $D_{eff} = D_{eff}^*$  for an isotropic structure) and in Eq. (7a),  $\varphi$  is the Thiele modulus defined as

$$\varphi = \sqrt{\frac{Ki a_v^*}{D_{eff}^*}} \quad (8)$$

where  $Ki$  is the kinetic number

$$Ki = \frac{k_0 \alpha_A \ell_R}{\mathcal{D}_A} \quad (9)$$



## 151 4.1 Hybrid model

When  $L_e^*/R_1^* \ll 1$ , Eq. (7a) can be simplified to the following form

$$\frac{d^2 \langle c_A^* \rangle^f}{dr^{*2}} - \varphi^2 \langle c_A^* \rangle^f = 0, \quad R_1^* \leq r^* \leq R_2^* \quad (10)$$

In the absence of any other assumption (in particular if  $L_e^* + L_N^*$  is not assumed to be exceedingly small compared to  $R_1^*$ ), Eqs. (7b) to (7f) remain unchanged. This yields the hybrid model which solution is given by<sup>[17]</sup>

$$\langle c_A^* \rangle^f = a_1 \cosh(\varphi(r^* - R_1^*)) \quad R_1^* \leq r^* \leq R_2^* \quad (11a)$$

$$c_A^* = b_1 \ln r^* + c_1 \quad R_2^* \leq r^* \leq R_3^* \quad (11b)$$

with

$$a_1 = (\mathbf{D}_{eff}^* \varphi \sinh(\varphi L_e^*) R_2^* \ln(R_3^*/R_2^*) + \cosh(\varphi L_e^*))^{-1} \quad (12a)$$

$$b_1 = \left( \frac{\coth(\varphi L_e^*)}{\mathbf{D}_{eff}^* R_2^* \varphi} + \ln(R_3^*/R_2^*) \right)^{-1} \quad (12b)$$

$$c_1 = 1 - b_1 \ln(R_3^*) \quad (12c)$$

Moreover, the current per unit volume can be expressed as

$$\frac{I}{V_e} = - \frac{nFk_0 \alpha_A a_v c_A^0}{\varphi L_e^* [\coth(\varphi L_e^*) + \mathbf{D}_{eff}^* \varphi R_2^* \ln(R_3^*/R_2^*)]} \quad (13)$$

152 where  $V_e$  is the volume of the electrode immersed in the reactive solution, *i.e.*,  
153 the active electrode volume.

## 154 4.2 Complete solution

155 At this point, no special hypothesis is made on the electrode dimensions and Eqs.  
156 (7) are kept as such. The solution of Eq. (7a) is given by a linear combination  
157 of the modified zeroth order Bessel's functions of the first and second kinds,  $I_0$   
158 and  $K_0$ , as<sup>[25]</sup>

$$\langle c_A^* \rangle^f = A_1 I_0(\varphi r^*) + B_1 K_0(\varphi r^*), \quad R_1^* \leq r^* \leq R_2^* \quad (14)$$

159 The coefficients  $A_1$  and  $B_1$  can be determined by making use of the boundary  
160 conditions (7c), (7d), (7e) and (7f). When this conditions are used, one obtains

161

$$A_1 = - \frac{K_1(\varphi R_1^*)}{I_1(\varphi R_1^*)} B_1 \quad (15a)$$

$$B_1 = \left[ - \frac{K_1(\varphi R_1^*)}{I_1(\varphi R_1^*)} I_0(\varphi R_2^*) + K_0(\varphi R_2^*) + \mathbf{D}_{eff}^* \varphi R_2^* \ln \frac{R_3^*}{R_2^*} \left( - \frac{K_1(\varphi R_1^*)}{I_1(\varphi R_1^*)} I_1(\varphi R_2^*) - K_1(\varphi R_2^*) \right) \right]^{-1} \quad (15b)$$

162 where  $I_1$  and  $K_1$  are the first order modified Bessel's functions of the first and  
 163 second kinds, respectively.

In the external diffusion layer, the concentration is given by

$$c_A^* = A_2 \ln r^* + B_2, \quad R_2^* \leq r^* \leq R_3^* \quad (16)$$

with

$$A_2 = \frac{1}{\ln(R_2^*/R_3^*)} (A_1 I_0(\varphi R_2^*) + B_1 K_0(\varphi R_2^*) - 1) \quad (17a)$$

$$B_2 = 1 - A_2 \ln R_3^* \quad (17b)$$

164 When the solution given in Eq.(14) is introduced in Eq. (6), the current per  
 165 unit active electrode volume,  $V_e$ , takes the following expression

$$\begin{aligned} \frac{I}{V_e} &= -\frac{C}{R_2^{*2} - R_1^{*2}} \int_{R_1^*}^{R_2^*} [A_1 I_0(\varphi r^*) + B_1 K_0(\varphi r^*)] r^* dr^* \\ &= -\frac{C}{R_2^{*2} - R_1^{*2}} (A_1 F_1 + B_1 F_2) \end{aligned} \quad (18)$$

with  $C$ ,  $F_1$  and  $F_2$  respectively given by

$$C = 2nk_0 F a_v \alpha_A c_A^0 \quad (19a)$$

$$F_1 = \int_{R_1^*}^{R_2^*} I_0(\varphi r^*) r^* dr^* = \frac{1}{\varphi} (R_2^* I_1(\varphi R_2^*) - R_1^* I_1(\varphi R_1^*)) \quad (19b)$$

$$F_2 = \int_{R_1^*}^{R_2^*} K_0(\varphi r^*) r^* dr^* = \frac{1}{\varphi} (R_1^* K_1(\varphi R_1^*) - R_2^* K_1(\varphi R_2^*)) \quad (19c)$$

166 In the following, numerical evaluation of the above solution on the current  
 167 versus the scanning potential is compared to that of the hybrid model. The  
 168 parameters used to compute these solutions are given in Table. 1. They cor-  
 169 respond to those used for the validation of the macroscopic model with direct  
 170 numerical simulations of the microscale model and experimental data.<sup>[7,17]</sup> The  
 171 electrochemical reaction considered here is typically the reduction of  $H_2O_2$  to  
 172  $H_2O$ . Moreover, the face-centered cubic (FCC) structure is assumed as the pe-  
 173 riodic REV of the porous medium constitutive of the electrode (see Fig. 2).  
 174 This structure is uniquely defined by the sphere diameter,  $d_s \equiv \ell_p$ , and the pore  
 175 connection window size,  $d_c$ .<sup>[7]</sup> The REV of the FCC structure corresponds to 4  
 176 half-layers (HL) of spherical pores.

177 The current versus the potential obtained from both the hybrid model and  
 178 Bessel's solution is represented in Fig. 4(a) for three different electrodes made  
 179 of 5HL, 15HL and 30HL of pores. As can be observed from this figure, the two  
 180 solutions are almost identical when the potential is sufficiently large, although  
 181 the hybrid model tends to underestimate the magnitude of the current. The  
 182 discrepancy between the two models becomes significant below a threshold value  
 183 of the potential which increases with the electrode thickness. This is made clear

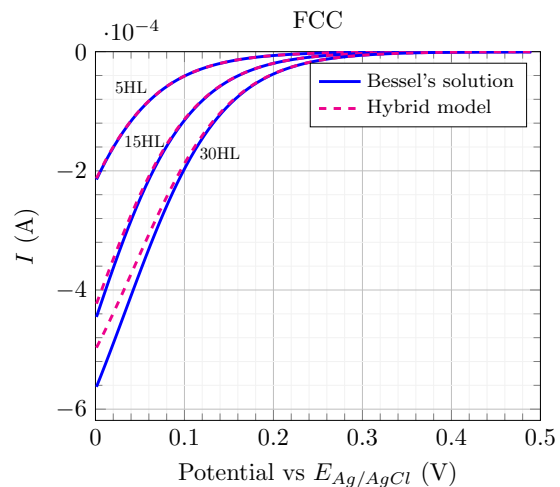
Table 1 – Parameters used for the solutions of the hybrid and complete models.

Parameter <sup>[7,17]</sup>	Symbol	Value	Unit
Ideal gas constant	$R$	8.314	J.mol <sup>-1</sup> .K <sup>-1</sup>
Faraday's constant	$F$	96485	C.mol <sup>-1</sup>
Number of electron transferred	$n$	2	–
Electron transfer coefficient	$\alpha$	0.482	–
Standard rate constant	$k_0$	$1.7 \times 10^{-17}$	cm.s <sup>-1</sup>
Standard potential vs. $E_{Ag/AgCl}^0$	$E_0$	1.56	V
Temperature	$T$	298	K
Bulk concentration	$c_A^0$	10	mol.m <sup>-3</sup>
Diffusion coefficient	$\mathcal{D}_A$	$10^{-9}$	m <sup>2</sup> .s <sup>-1</sup>
Spherical pore diameter	$d_s = \ell_p$	1.17	$\mu\text{m}$
Pore connection window size	$d_c$	$0.15d_s$	m
Size of the periodic unit cell	$\ell_R$	1.64	$\mu\text{m}$
Porosity	$\varepsilon_f$	0.763	–
Specific surface area	$a_v$	$3.567 \times 10^6$	m <sup>-1</sup>
Normalized effective coefficient	$D_{eff}^*$	0.364	–
Wire radius	$R_1$	25	$\mu\text{m}$
Diffusion layer thickness	$L_N$	100	$\mu\text{m}$

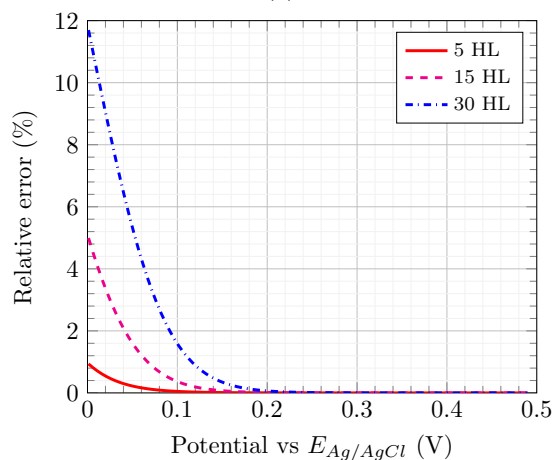
184 in Fig. 4(b) representing the absolute value of the relative error between the two  
 185 models (the Bessel's solution is taken as the reference) showing that this relative  
 186 error can reach about 12 % for the thickest electrode under consideration when  
 187 the potential is close to 0V.

188 Numerical simulations on other microstructures, namely cubic (C) and body-  
 189 centered cubic (BCC) which unit cells are represented in Fig. 5, are also carried  
 190 out using the parameters given in Table 1. The resulting values of  $\varepsilon$ ,  $a_v$ ,  $D_{eff}^*$  and  
 191  $\ell_R$  are reported in Table 2. In Fig. 6, the current versus the scanning potential  
 192 obtained for different electrode thicknesses computed with the complete solution  
 193 and the hybrid model are represented for the C (Fig. 6(a)) and BCC (Fig. 6(b))  
 194 structures. As already observed for the FCC structure, a significant difference  
 195 between the two models exists in particular for a thick electrode, and this is a  
 196 general feature for any microstructure. Again, the hybrid model accuracy fails  
 197 when the thickness to inner radius ratio is not small enough compared to 1.

198 The analysis can now be focused on the optimal electrode thickness using  
 199 the same approach as the one recently investigated.<sup>[17]</sup> To begin with, it is  
 200 instructive to illustrate the electrode efficiency with the reagent concentration  
 201 profile. In Fig. 7  $\langle c_A^* \rangle^f$  obtained from Eq. (14) with  $L_e^*$  and parameters of Table  
 202 (1) is represented within the electrode ( $R_1^* < r^* < R_2^*$ ) for  $Ki = 10^{-4}$  and  $Ki =$   
 203  $10^{-3}$ . This figure clearly shows that the penetration depth of the concentration  
 204 front inside the electrode decreases as the kinetic number increases, *i.e.* when  
 205 reaction becomes more significant so that species  $A$  is consumed in the vicinity of  
 206 the electrode/diffusion layer interface. As a result, a large part of the electrode



(a)



(b)

Figure 4 – (a) Current versus the scanning potential obtained from the hybrid model and Bessel’s solution for the 5HL, 15HL and 30 HL electrodes. (b) Absolute value of the relative error between the two solutions taking the Bessel’s solution as the reference.

207 (about half of it in Fig. 7 for  $Ki = 10^{-3}$ ), in the region far enough from this  
 208 interface, does not contribute much to the current production. This observation  
 209 is an evidence that an optimal thickness can be determined and this is carried  
 210 out as follows.

The current per unit volume expressed in Eq. (18) decreases with the electrode thickness,  $L_e^*$ , in two characteristic regimes (see Fig. 8): a rapid decrease

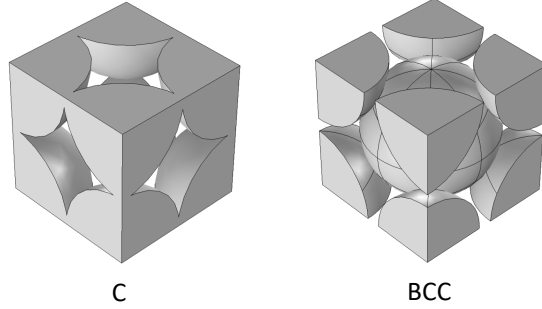


Figure 5 – Unit cell of the C and BCC structures.

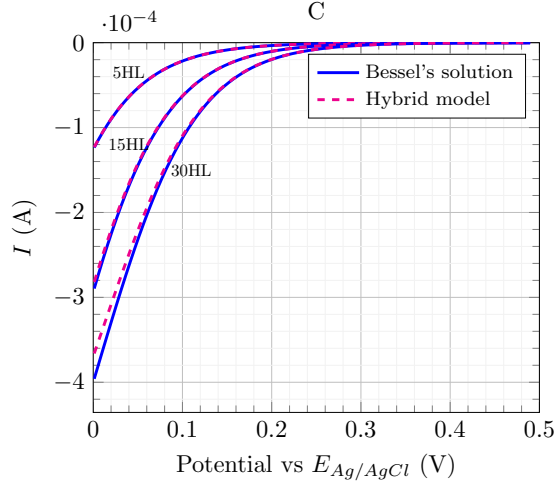
Table 2 – Properties of C and BCC structures used in the simulations.

Parameter <sup>[7]</sup>	Symbol	Value	Unit
C			
Porosity	$\varepsilon_f$	0.541	–
Specific surface area	$a_v$	$2.68 \times 10^6$	$\text{m}^{-1}$
Normalized effective diffusion coefficient	$D_{eff}^*$	0.142	–
Size of the periodic unit cell	$\ell_R$	1.16	$\mu\text{m}$
BCC			
Porosity	$\varepsilon_f$	0.703	–
Specific surface area	$a_v$	$3.44 \times 10^6$	$\text{m}^{-1}$
Normalized effective diffusion coefficient	$D_{eff}^*$	0.236	–
Size of the periodic unit cell	$\ell_R$	1.34	$\mu\text{m}$

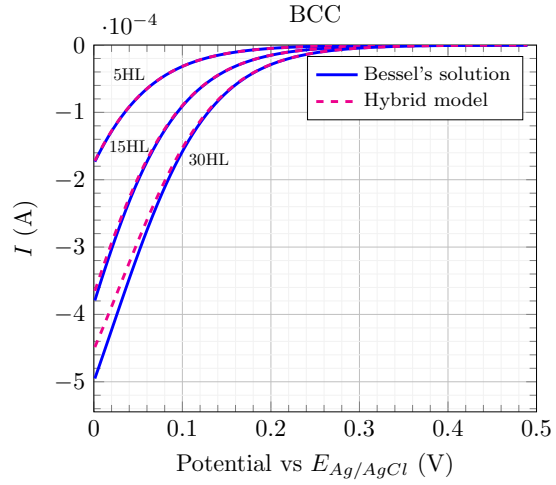
at small electrode thicknesses followed by a slow convergence to zero at very large values of  $L_e^*$ . This suggests defining the optimal thickness,  $L_e^{*op}$ , as the crossover between these two regimes. Practically, this value is obtained at the intersecting point of the tangent to  $|I/V_e|$  at  $L_e^{*0}$  with  $|I/V_e|=0$ . The value of  $L_e^{*0}$  should be taken as the minimum thickness that is experimentally achievable, *i.e.*,  $L_e^{*0} \geq 1$ . The value of  $L_e^{*op}$  can hence be obtained from the following expression

$$L_e^{*op} = - \frac{|I/V_e|_{L_e^{*0}}}{\left. \frac{\partial |I/V_e|}{\partial L_e^*} \right|_{L_e^{*0}}} + L_e^{*0} \quad (20)$$

The derivative of the current per unit volume with respect to  $L_e^*$  involved in this last relationship can be determined analytically from Eq. (18). It is given



(a)



(b)

Figure 6 – Current versus the scanning potential obtained from the hybrid model and Bessel's solution for the 5HL, 15HL and 30 HL electrodes: (a) cubic structure (C) (b) body-centered cubic structure (BCC).

by

$$\frac{\partial(|I/V_e|)}{\partial L_e^*} = \frac{2R_2^*}{R_2^{*2} - R_1^{*2}} \frac{I}{V_e} + \frac{C}{R_2^{*2} - R_1^{*2}} \left( \frac{\partial A_1}{\partial L_e^*} F_1 + \frac{\partial B_1}{\partial L_e^*} F_2 + R_2^* \langle c_A^* \rangle^f \Big|_{R_2^*} \right) \quad (21)$$

211 As a result, the optimal electrode thickness can be estimated analytically once  
 212 the electrode features are provided, namely  $\ell_R$ ,  $a_v^*$ ,  $D_{eff}^*$  and  $R_1^*$ . Once these

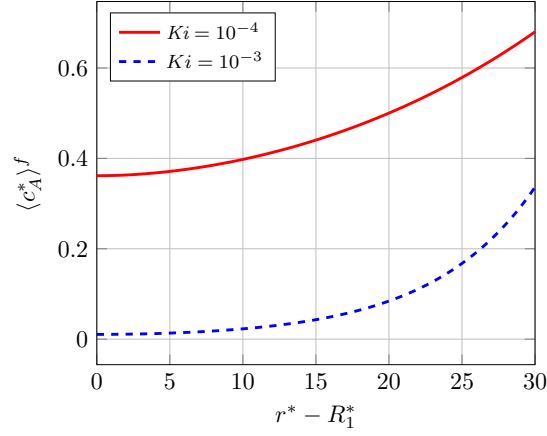


Figure 7 – Normalized concentration profile of species  $A$  in the electrode for two values of the kinetic number. The dimensionless electrode thickness is  $L_e^* = 30$  the other parameters being those in Table 1.

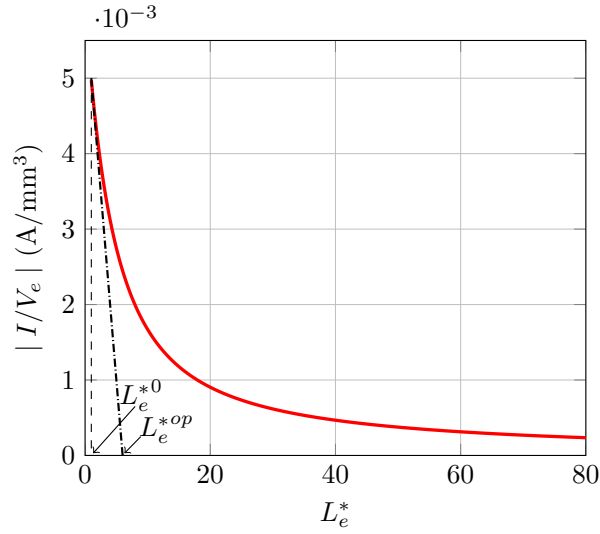


Figure 8 – Variation of the current per unit volume,  $|I/V_e|$ , obtained from Eq. (18) versus the electrode's dimensionless thickness,  $L_e^*$ , in the case of a FCC microstructure for  $Ki = 10^{-3}$  and  $L_N = 100\mu\text{m}$ . The other parameters used to compute the current per unit volume are provided in Table 1. The optimal thickness,  $L_e^{*op}$ , is obtained from the intersection of the tangent to this graph at  $L_e^* = L_e^{*0}$  with the axis  $|I/V_e| = 0$ . See text for the details.

213 porous medium properties are fixed, the value of  $L_e^{*op}$  can be computed as it  
 214 only depends on the conditions at which it is supposed to operate, *i.e.*,  $Ki$

215 and  $L_N^*$ . In the case of the FCC structure considered so far, and with the  
 216 parameters reported in Table 1, together with  $L_e^{*0} = 1$ ,  $L_e^{*op}$  was computed  
 217 from Eq. (20) for  $Ki$  values up to  $2 \times 10^{-3}$ . The corresponding results are  
 218 reported in Fig. 9(a) considering two values of the diffusion layer thickness,  
 219 namely  $L_N = 100\mu\text{m}$  and  $L_N = 200\mu\text{m}$ . As expected,  $L_e^{*op}$  increases when  $L_N$   
 220 decreases. This is due to the fact that a thinner diffusion layer (*i.e.* imposing  
 221 a Dirichlet boundary condition closer to the fluid porous layer interface) allows  
 222 a more efficient penetration of the reagent inside the porous electrode so that  
 223 a thicker active layer is permitted. In addition, the optimal thickness obtained  
 224 with the hybrid model reported elsewhere<sup>[17]</sup> is also represented in this figure.

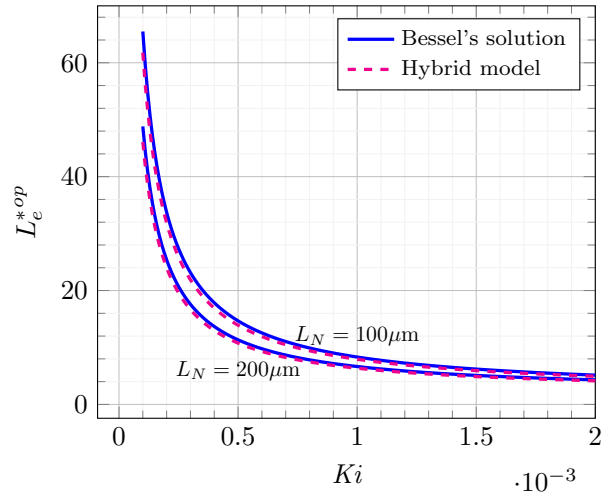
225 As can be observed on this figure, the difference between the predictions of  
 226 the two models remains very small. This is highlighted in Fig. 9(b) representing  
 227 the relative error between the two predictions, taking the Bessel's solution as  
 228 the reference. Indeed, the largest difference is for the smallest values of  $Ki$  (*i.e.*  
 229 for the largest values of  $E$ ) and small values of the diffusion layer thickness. For  
 230 the case under study, this difference does not exceed 6%.

231 These results show that the hybrid model remains robust if one is willing  
 232 to estimate the optimal thickness of the electrode although it can significantly  
 233 underestimate the current, in particular for the smallest values of the potential  
 234 when the condition  $2L_e^*/(R_1^* + R_2^*) \ll 1$  is not satisfied.

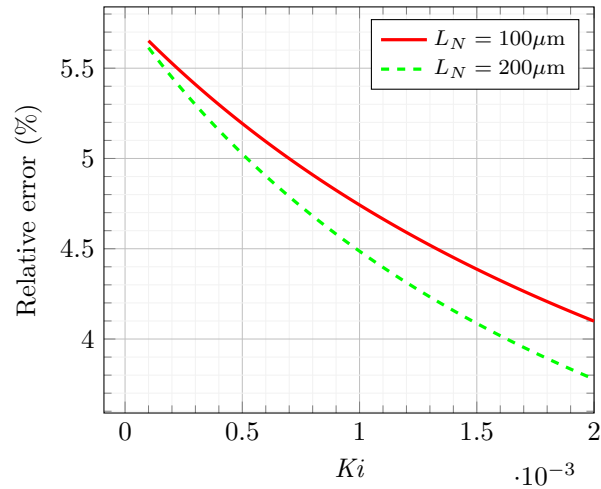
235 The normalized optimal thickness predicted for the other microstructures (C  
 236 and BCC), compared to the FCC structure, is represented in Fig. 10. Clearly,  
 237 the dependence of  $L_e^{*op}$  on  $Ki$  is similar whatever the structure. This brings to  
 238 the general conclusion that, whatever the microstructure, the optimal thickness  
 239 decreases rapidly with the kinetic number and tends to a constant value for large  
 240 values of  $Ki$ . Quantitatively, the comparison of the optimal thickness of the three  
 241 structures must be made with care as  $L_e^{*op}$  and  $Ki$  are based on  $\ell_R$  which is not  
 242 the same from one structure to another. For this purpose, a representation  
 243 where  $\ell_p = d_s$  (identical for C, BCC and FCC) is used as the reference length is  
 244 given in the inset of Fig. 10. It shows that the optimal thickness for the BCC  
 245 and FCC structures is almost the same (it is slightly larger for the former),  
 246 but is larger for the C structure. The physical explanation of this behavior  
 247 can be deduced after examining the reduced sensibility of  $L_e^{*op}$  to  $a_v$  and  $D_{eff}^*$   
 248 that are reported in Fig. 11. It should be noted that the reduced sensibility of  
 249  $L_e^{*op}$  to the parameter  $u$  is defined as  $u\partial L_e^{*op}/\partial u$ . This figure shows that the  
 250 reduced sensibility to  $a_v$  is negative (*i.e.*  $L_e^{*op}$  increases when  $a_v$  decreases) and  
 251 is much larger in magnitude than that to  $D_{eff}^*$ . Consequently, the contrast on  
 252  $L_e^{*op}$  between the three structures can be interpreted only considering  $a_v$ . Since  
 253  $a_v$  is not markedly different for the BCC and FCC structures (although slightly  
 254 smaller for the former) but significantly smaller for the C structure (see Tables  
 255 1 and 2), the expected variation of  $L_e^{*op}$  with respect to the structure is exactly  
 256 that observed in Fig. 10 and mentioned above.

257 Finally, it is of interest to investigate which structure, among the three  
 258 considered here, is the most efficient in terms of current production. Results  
 259 of the current per unit length,  $L$ , of the electrode at its optimal thickness are  
 260 represented in Fig. 12 for the C, BCC and FCC structures versus  $Ki$ . From this





(a)



(b)

Figure 9 – (a) Optimal thickness versus the kinetic number for two values of the diffusion layer thickness, obtained from the Bessel’s solution and hybrid model (b) Absolute relative error between the two approaches taking the values obtained with the Bessel’s solution as the reference. FCC structure. Parameters are those reported in Table 1.

261 figure, it can be readily concluded that the FCC structure produces the largest  
 262 current per unit length. In addition to the fact that it also allows the thinner  
 263 optimal thickness, this structure is the most advantageous one among the three  
 264 simple cases envisaged here. In what follows, results are only illustrated for a

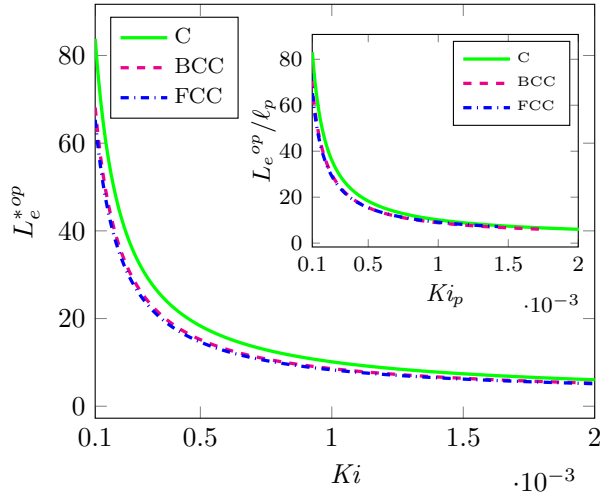


Figure 10 – Optimal thickness versus the kinetic number for C, BCC and FCC structures.  $L_N = 100\mu\text{m}$ . For all structures,  $d_c$  and  $d_s$  are the same (see Table 1) featuring different values of  $\varepsilon$ ,  $a_v$ ,  $D_{eff}^*$  and  $\ell_R$  (see the values in Table 1 for the FCC and in Table 2 for the C and BCC structures respectively). All other parameters are the same and are reported in Table 1. Inset:  $L_e^{*op}$  made dimensionless by the spherical pore diameter,  $\ell_p = d_s$ , versus the pore kinetic number,  $Ki_p = \frac{k_0 \alpha_A \ell_p}{D_A}$  for the three structures.

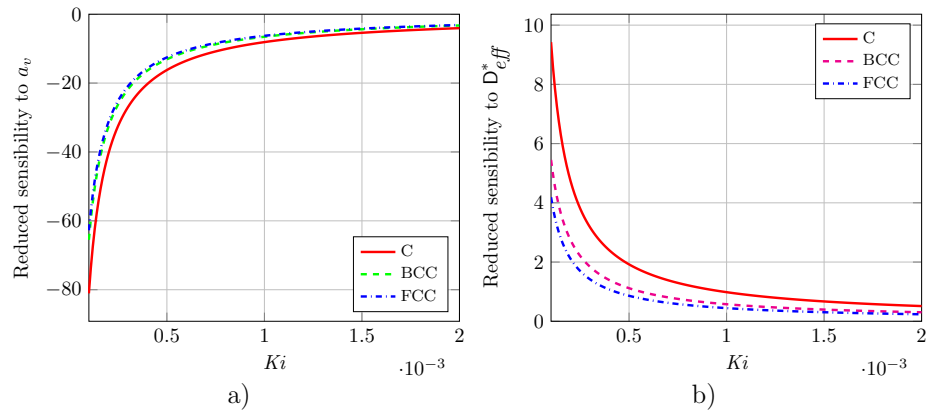


Figure 11 – Reduced sensibility of  $L_e^{*op}$  to a)  $a_v$  and b)  $D_{eff}^*$  for the three structures C, BCC and FCC.

265 FCC structure.

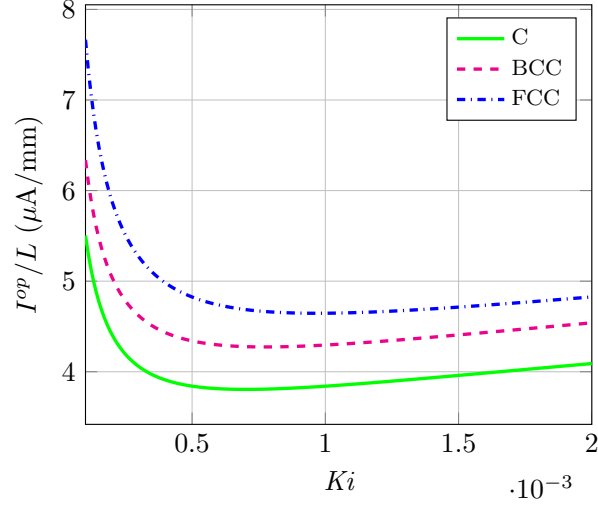


Figure 12 – Current per unit length,  $L$ , of the electrode at its optimal thickness for the three structures C, BCC and FCC versus  $Ki$ . Parameters are those reported in Table 1.

## 266 5 Planar electrode

For the sake of completeness, the case of a planar electrode is now investigated by providing the analytical solution for the current and optimal thickness. In this situation, the porous material is deposited onto a plane solid surface, as in the cases envisaged by Barnes *et al.*<sup>[15]</sup> and Cai *et al.*<sup>[26]</sup>, for instance. Assuming that the extension of the electrode in both directions of the plane are much larger than the electrode thickness, the model reduces to one dimension, in the  $z$ -direction orthogonal to the plane. Using the same dimensionless variables as in section 4, the problem can be formulated as follows

$$\frac{\partial^2 \langle c_A^* \rangle^f}{\partial z^{*2}} - \varphi^2 \langle c_A^* \rangle^f = 0 \quad 0 \leq z^* \leq L_e^* \quad (22a)$$

$$\frac{\partial}{\partial z^*} \left( \frac{\partial c_A^*}{\partial z^*} \right) = 0 \quad L_e^* \leq z^* \leq L_e^* + L_N^* \quad (22b)$$

$$\text{B.C.1} \quad \frac{\partial \langle c_A^* \rangle^f}{\partial z^*} = 0 \quad z^* = 0 \quad (22c)$$

$$\text{B.C.2} \quad \langle c_A^* \rangle^f = c_A^* \quad z^* = L_e^* \quad (22d)$$

$$\text{B.C.3} \quad D_{eff}^* \frac{\partial \langle c_A^* \rangle^f}{\partial z^*} = \frac{\partial c_A^*}{\partial z^*} \quad z^* = L_e^* \quad (22e)$$

$$\text{B.C.4} \quad c_A^* = 1 \quad z^* = L_e^* + L_N^* \quad (22f)$$

The analytical solution to the above system of equations is given by

$$\langle c_A^* \rangle^f = a_2 \cosh(\varphi z^*) \quad 0 \leq z^* \leq L_e^* \quad (23a)$$

$$c_A^* = b_2 z^* + c_2 \quad L_e^* \leq z^* \leq L_e^* + L_N^* \quad (23b)$$

where the coefficients  $a_2$ ,  $b_2$  and  $c_2$  have the following expressions

$$a_2 = [\cosh(\varphi L_e^*) + D_{eff}^* \varphi L_N^* \sinh(\varphi L_e^*)]^{-1} \quad (24a)$$

$$b_2 = \left[ \frac{\coth(\varphi L_e^*)}{D_{eff}^* \varphi} + L_N^* \right]^{-1} \quad (24b)$$

$$c_2 = 1 - b_2(L_e^* + L_N^*) \quad (24c)$$

Using Eq. (23a) in Eq. (6), the current per unit volume,  $V_e$ , can be written as

$$I/V_e = - \frac{n F k_0 \alpha_A a_v c_A^0}{\varphi L_e^* [\coth(\varphi L_e^*) + D_{eff}^* \varphi L_N^*]} \quad (25)$$

Its derivative with respect to  $L_e^*$  can then be expressed as

$$\frac{\partial |I/V_e|}{\partial L_e^*} = - \frac{n F k_0 \alpha_A a_v c_A^0}{\varphi} \frac{\varphi (1 - \coth^2(\varphi L_e^*)) L_e^* + \coth(\varphi L_e^*) + D_{eff}^* \varphi L_N^*}{[\coth(\varphi L_e^*) L_e^* + D_{eff}^* \varphi L_N^* L_e^*]^2} \quad (26)$$

267 From these two last relationships, the optimal thickness can be determined  
 268 by making use of Eq. (20). The results of this prediction is represented in Fig.  
 269 13 considering a FCC structure,  $L_N = 100 \mu\text{m}$ ,  $L_e^{*0} = 1$  and  $Ki$  up to  $2 \times 10^{-3}$ ,  
 all the other parameters being those reported in Table 1. As a validation,

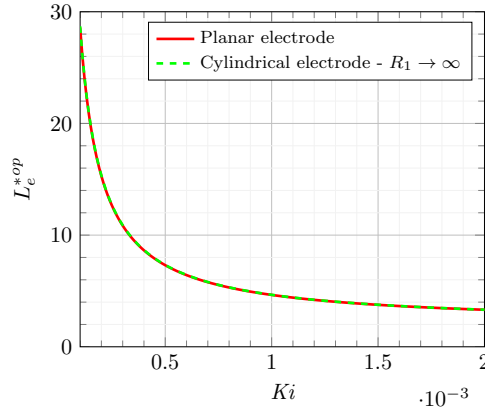


Figure 13 – Optimal thickness versus the kinetic number obtained for planar electrode and cylindrical electrode taking  $R_1 \rightarrow \infty$ .  $L_N = 100 \mu\text{m}$ . FCC structure. All the parameters are those reported in Table 1.

271 the solution of the complete model in the limit  $R_1 \rightarrow \infty$  is also reported in  
 272 this figure, showing that, in this limit, the two predictions perfectly match, as  
 273 expected. This confirms that the complete solution is a general one, whatever  
 274 the electrode dimensions. On the basis of this general result, the analysis can  
 275 be carried on to determine the optimal radius,  $R_1^{*op}$ , of the supporting wire and  
 276 this is the objective of the following section.

## 277 6 Optimal wire radius, $R_1^{*op}$

278 A comparison of the results reported in Fig. 13 with those in Fig. 9(a) indicates  
 279 that, all parameters being the same, the optimal thickness of the planar electrode  
 280 is smaller than that of a cylindrical electrode having a finite radius. The contrast  
 281 between the two is more significant when  $Ki$  decreases. This suggests to further  
 282 analyze the dependence of  $L_e^{*op}$  upon the wire radius,  $R_1^*$ , for a given set of the  
 283 physico-chemical parameters. More particularly, it is of interest to investigate  
 284 the variation of the volume (per unit length,  $L$ ) of the electrode at its optimal  
 285 thickness,  $V_e^{op}/L$ , with respect to  $R_1^*$ . Such a variation is illustrated in Fig.  
 286 14, considering two values of  $Ki$ , namely  $Ki = 5 \cdot 10^{-4}$  and  $Ki = 10^{-3}$ , taking  
 287  $L_N = 100\mu\text{m}$ , all other parameters being those reported in Table 1 and a FCC  
 structure.

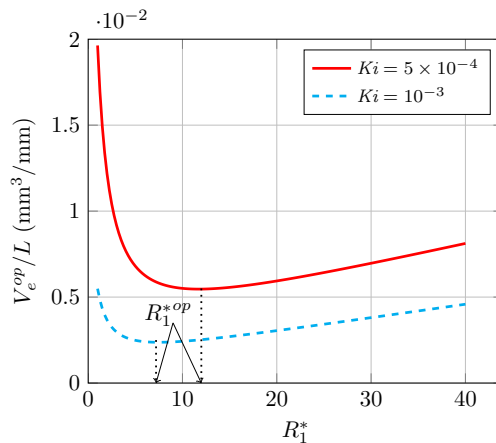


Figure 14 – Variation of the volume (per unit length,  $L$ ) of the electrode at its optimal thickness,  $V_e^{op}/L$ , versus the dimensionless wire radius,  $R_1^*$ , for  $Ki = 5 \cdot 10^{-4}$  and  $Ki = 10^{-3}$ , taking  $L_N = 100\mu\text{m}$  (see Table 1 for the other parameters). FCC structure.

288  
 289 This figure clearly shows that  $V_e^{op}/L$  exhibits a minimum which means that  
 290 there exists a particular value of  $R_1^*$ , denoted  $R_1^{*op}$ , which minimizes the volume  
 291 of material necessary to achieve the optimal thickness. This is extremely im-  
 292 portant keeping in mind that the porous medium is usually made of expensive  
 293 materials using complex procedures. In Fig. 15,  $R_1^{*op}$  is represented versus  $Ki$

in the range  $10^{-4} \leq Ki \leq 10^{-3}$  for  $L_N = 100\mu\text{m}$ . As can be seen on this graph,

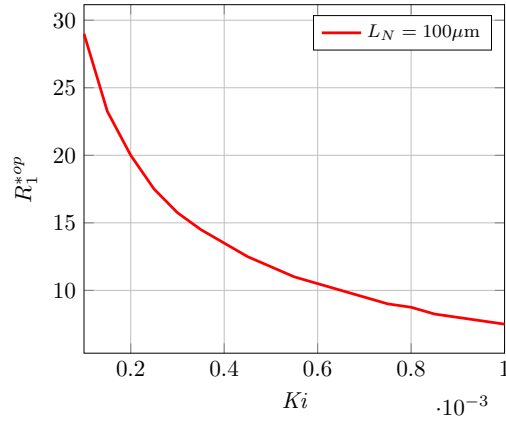


Figure 15 – Variation of the dimensionless optimal wire radius,  $R_1^{*op}$ , versus  $Ki$  for  $L_N = 100\mu\text{m}$  (see Table 1 for the other parameters). FCC structure.

294

295

296

the optimal wire radius decreases when  $Ki$  increases. Moreover,  $R_1^{*op}$  seems to very weakly depend on  $L_N$ , as indicated by Fig. 16 where  $R_1^{*op}$  is represented versus  $L_N$  ranging from  $100\mu\text{m}$  to  $400\mu\text{m}$  for  $Ki = 5 \cdot 10^{-4}$  and  $Ki = 10^{-3}$ . This

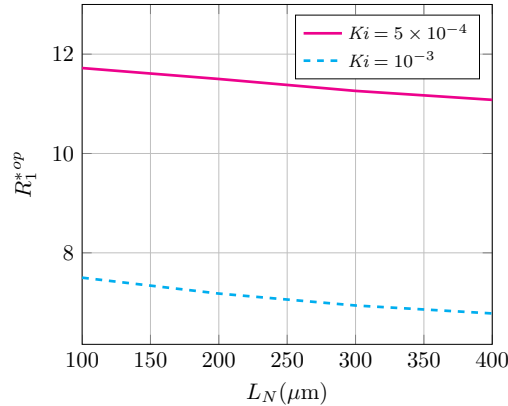


Figure 16 – Variation of the dimensionless optimal wire radius,  $R_1^{*op}$ , versus  $L_N$  for  $Ki = 5 \cdot 10^{-4}$  and  $Ki = 10^{-3}$  (see Table 1 for the other parameters). FCC structure.

297

298

299

300

301

302

suggests that the value of  $R_1^{*op}$  can be determined regardless the value of  $L_N$ , *i.e.* as only a function of  $Ki$  when the microstructural parameters are fixed.

This last analysis completes the optimization procedure of the electrode macroscopic dimensions as its thickness and supporting wire diameter can be predicted in order to obtain the optimal current per unit volume when the

303 operating conditions and the microstructure of the porous material are known.  
304 This represents a major result of this work.

## 305 **7 Conclusion**

306 In this work, steady-state solutions of the macroscopic model describing the  
307 coupled process of electrochemical heterogeneous reaction and diffusion are de-  
308 veloped for cylindrical and planar porous micro-electrodes.

309 The complete solution developed here provides a more accurate prediction  
310 of the current delivered by the electrode versus the applied potential than the  
311 hybrid model reported earlier which is recovered in the limit of a thickness to  
312 inner radius ratio much smaller than unity and which remains valid in this  
313 limit. Moreover, the complete solution also matches the one developed in the  
314 case of a planar electrode in the limit of exceedingly large radii. This makes the  
315 complete solution a general one, whatever the dimensions and microstructure  
316 of the electrode, the characteristics of the latter being reflected in the porosity,  
317 specific area and effective diffusion coefficient. The use of this complete solution  
318 is strongly recommended particularly when the constraint on the dimensions is  
319 not satisfied.

320 More importantly, it is shown that an optimal radius of the supporting wire  
321 exists for a given set of the physico-chemical parameters defining the operating  
322 conditions of the electrode. This optimal radius is derived as to satisfy the  
323 minimum volume of the porous material required to ensure the optimal current  
324 per unit volume. This represents a salient result of the present work.

325 Together with the prediction of the current delivered by the electrode, the  
326 solution derived here allows for the determination of the electrode optimal di-  
327 mensions in terms of its thickness and inner radius. This provides a complete  
328 and effective operational procedure of optimization of the macroscopic char-  
329 acteristics of cylindrical electrodes operating a single reduction reaction as a  
330 predictive tool for their practical design. As a final remark, it should be noticed  
331 that the approach developed here may be advantageously employed for the opti-  
332 mal design of other electrochemical devices devoted to energy production which  
333 architecture and operating conditions share similarities with those envisaged in  
334 this work.

## 335 **8 Acknowledgment**

336 This work was supported by the ANR project MOMA (ANR-17-CE08-0005).

## 337 **9 Keywords**

338 Porous micro-electrode, Optimal thickness, Optimal radius, Analytical solution,  
339 Volume averaging method

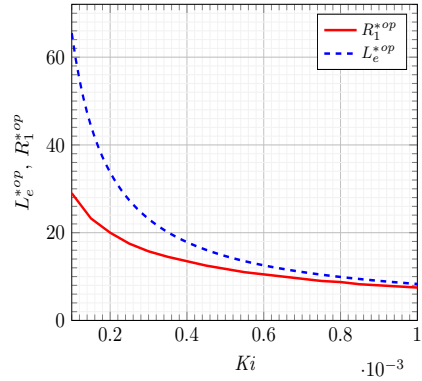
## 340 References

- 341 [1] A. Zebda, J. Alcaraz, P. Vadgama, S. Shleev, S. D. Minteer, F. Boucher,  
342 P. Cinquin, and D. K. Martin, *Bioelectrochemistry* **2018**, 124, 57–72.
- 343 [2] A. Walcarius and A. Kuhn, *Trends Anal. Chem.* **2008**, 27, 593–603.
- 344 [3] D. Leech, P. Kavanagh, and W. Schuhmann, *Electrochim. Acta* **2012**, 84,  
345 223–234.
- 346 [4] S. Cosnier, A. J. Gross, A. L. Goff, and M. Holzinger, *J. Power Sources*  
347 **2016**, 325, 252–263.
- 348 [5] S. Shleev, *ChemPlusChem* **2017**, 82, 522–539.
- 349 [6] M. Gamella, A. Koushanpour, and E. Katz, *Bioelectrochemistry* **2018**, 119,  
350 33–42.
- 351 [7] T. D. Le, D. Lasseux, X. P. Nguyen, G. L. Vignoles, N. Mano, and A. Kuhn,  
352 *Chem. Eng. Sci.* **2017**, 173, 153–167.
- 353 [8] T. D. Le, L. Zhang, A. Kuhn, N. Mano, G. L. Vignoles, and D. Lasseux,  
354 *J. Electroanal. Chem.* **2019**, 855, 113325.
- 355 [9] T. Q. N. Do, M. Varničić, R. Hanke-Rauschenbach, T. Vidaković-Koch,  
356 and K. Sundmacher, *Electrochim. Acta* **2014**, 137, 616–626.
- 357 [10] T. Q. N. Do, M. Varničić, R. Flassig, T. Vidaković-Koch, and K. Sund-  
358 macher, *Bioelectrochemistry* **2015**, 106, 3–13.
- 359 [11] S. Reculosa, M. Heim, F. Gao, N. Mano, S. Ravaine, and A. Kuhn, *Adv.*  
360 *Funct. Mater.* **2011**, 21(4), 691–698.
- 361 [12] A. Karajić, S. Reculosa, M. Heim, P. Garrigue, S. Ravaine, N. Mano, and  
362 A. Kuhn, *Adv. Mater. Interfaces*, vol. 2, no. 12, pp. 1500192–1500196, 2015.
- 363 [13] R. D. Levie, *Adv. Electrochem. Electrochem. Eng.* **1967**, 6, 329–397.
- 364 [14] O. E. Barcia, E. D’Elia, I. Frateur, O. R. Mattos, N. Pebere, and B. Tri-  
365 bollet, *Electrochim. Acta* **2002**, 47, 2109–2116.
- 366 [15] E. O. Barnes, X. Chen, P. Li, and R. G. Compton, *J. Electroanal. Chem.*  
367 **2014**, 720–721, 92–100.
- 368 [16] D. Zhang, A. Bertei, F. Tariq, N. Brandon, and Q. Cai, *Prog. Energy* **2019**,  
369 1, 012003, 2019.
- 370 [17] T. D. Le, L. Zhang, G. L. Vignoles, N. Mano, A. Kuhn, and D. Lasseux,  
371 *ChemElectroChem* **2019**, 6, 173–180.
- 372 [18] A. Fick, *J. Membr. Sci.* **1995**, 100, 33–38.



- 373 [19] S. Whitaker, *Rev. Mex. Ing. Chim.* **2009**, 8, 213–243.
- 374 [20] J. A. V. Butler, *Trans. Faraday Soc.* **1924**, 19, 729–733.
- 375 [21] S. Whitaker, *The Method of Volume Averaging*. Dordrecht, The Netherlands: Kluwer Academic Publishers, 1999.
- 377 [22] J. C. Slattery, *Advanced Transport Phenomena (Cambridge Series in*  
378 *Chemical Engineering)*. Cambridge University Press, 1999.
- 379 [23] F. Howes and S. Whitaker, *Chem. Eng. Sci.* **1985**, 40, 1387–1392.
- 380 [24] W. Gray, *Chem. Eng. Sci.*, vol. 30, pp. 229–233, 1975.
- 381 [25] A. D. Polyanin and V. F. Zaitsev, *Handbook of Exact Solutions for Ordinary*  
382 *Differential Equations*. Chapman and Hall/CRC, 3rd Ed., 2003.
- 383 [26] Q. Cai, C. S. Adjiman, and N. P. Brandon, *Electrochim. Acta* **2011**, 56,  
384 10809–10819.

385 **Graphical abstract**



**Normalized optimal thickness,  $L_e^{*op}$ , and optimal supporting wire radius,  $R_1^{*op}$ , of a cylindrical electrode as a function of the kinetic number,  $Ki$  (diffusion layer thickness:  $L_N = 100\mu m$ ).**

386 A complete solution of the diffusion/reaction macroscopic problem govern-  
 387 ing the current production of a cylindrical porous electrode is developed. The  
 388 solution is used to predict the optimal thickness of the electrode and its op-  
 389 timal inner radius corresponding to the best compromise between a minimum  
 390 electrode volume and a maximum current per unit volume. This work provides  
 391 a complete optimization procedure that can be used as predictive tools for the  
 392 design of porous electrode.